

Posterior Atrophy is a Neuroimaging Marker of Mild Cognitive Impairment in Parkinson's Disease

Ulaş AY^{1,2}, Zerrin YILDIRIM^{3,4}, Ani KİCİK⁵, Emel ERDOĞDU⁶, Başar BİLGİÇ⁷, Hasmet HANAGASI⁷,
Esin OZTURK-ISIK⁸, Tamer DEMİRALP^{1,2}, Hakan GURVİT⁷

¹Istanbul University, Hulusi Behçet Life Sciences Research Center, Neuroimaging Unit, Istanbul, Türkiye

²Istanbul University, Istanbul Faculty of Medicine, Department of Physiology, Istanbul, Türkiye

³Istanbul University, Aziz Sançar Institute of Experimental Medicine, Department of Neuroscience, Istanbul, Türkiye

⁴University of Health Sciences, Bağcılar Training and Research Hospital, Department of Neurology, Istanbul, Türkiye

⁵Demiroğlu Bilim University, Faculty of Medicine, Department of Physiology, Istanbul, Türkiye

⁶Isik University, Faculty of Arts and Sciences, Department of Psychology, Istanbul, Türkiye

⁷Istanbul University, Istanbul Faculty of Medicine, Department of Neurology, Behavioral Neurology and Movement Disorders Unit, Istanbul, Türkiye

⁸Bogazici University, Institute of Biomedical Engineering, Istanbul, Türkiye

ABSTRACT

Introduction: Although there are several studies on the neuroanatomical mechanisms underlying Parkinson's disease (PD)-associated cognitive impairment, the clinical usefulness of the findings from these investigations is limited. In this study, we aimed to identify magnetic resonance imaging (MRI) markers that can be practically utilized for diagnosing PD-associated cognitive impairment using a visual rating scale (VRS).

Methods: Anatomical MRIs of cognitively normal (PD-CN), and PD with mild cognitive impairment (PD-MCI) patients were visually evaluated for six bilateral cortical regions. Then, hypothesis-driven cortical thickness analysis (CTA) was performed in the regions obtained from VRS.

Results: As a consequence of VRS, a significant difference was found

between the two groups with regards to right posterior atrophy (PA) scores (pFDR-corr = 0.042, Cohen's d= 1.06). Hypothesis-driven CTA confirmed the result of VRS by revealing cortical thinning at the precuneus and parieto-occipital sulcus junction (Max. T= 6.171, P= 0.0006, MNI_{x,y,z} = 11.0, -62.2, 25.4). The area under the curve was 0.75, showing a good association between the PD-MCI and the right PA score. The cut-off for maximum accuracy was ≥ 2 , based on the highest sum of sensitivity (0.68) and specificity (0.72).

Conclusions: Our findings indicate that right PA atrophy may be helpful for clinicians in the diagnosis of PD-associated cognitive impairment.

Keywords: Cortical thinning, Parkinson's disease, Parkinson's disease with mild cognitive impairment, posterior atrophy, visual rating scale

Cite this article as: Ay U, Yıldırım Z, Kıcık A, Erdoğan E, Bilgiç B, Hanagasi H, et al. Posterior Atrophy is a Neuroimaging Marker of Mild Cognitive Impairment in Parkinson's Disease. Arch Neuropsychiatry 2026;63:137-143. doi: 10.29399/npa.28821

INTRODUCTION

Parkinson's disease (PD) is the second most common neurodegenerative disorder (1). Although it is classically defined with motor symptomatology, such as bradykinesia, rigidity, and tremor, it is now known that there is also a wide range of non-motor symptoms (NMS) that can be seen from the earliest stages of the disease and some of which may precede motor symptoms (2). NMS of PD consists of dysautonomia, including chronic constipation, mood changes including depression and anxiety, parasomnia (REM-sleep behavior disorder), hyposmia, and cognitive impairment. The temporal pattern of the emergence of NMS is best explained by Braak's caudo-rostral spread staging of Lewy bodies (LBs), the causative neurodegenerative aggregate in PD (3). Accordingly, constipation and anosmia correspond to stage 1, the initial emergence of the LBs synchronously within the lower brainstem and olfactory system (dorsal motor nucleus of the vagus nerve and the olfactory bulbs). This is followed by the involvement of pontine structures in stage 2, resulting in mood changes and parasomnia. Current diagnostic criteria of PD can finally be fulfilled in stage 3 with the involvement of the dopaminergic substantia nigra pars compacta in the upper brainstem, leading to

Highlights

- Mild cognitive impairment is prevalent in Parkinson's disease (PD-MCI).
- The structural neuroimaging markers for PD-MCI remain ambiguous.
- The posterior atrophy (PA) determined by visual rating could be a PD-MCI marker.
- Visual rating and automated algorithms agree on PA presence in PD-MCI.

dopaminergic deafferentation of dorsal striatum including the motor circuit, giving rise to asymmetric bradykinesia typical of the so-called Parkinsonism. However, the deafferentation of the parallel dorsolateral prefrontal circuit logically gives rise to cognitive impairment in the form of

a dysexecutive syndrome synchronously with motor symptoms. Cortical involvement starts in stage 4 with the involvement of the allocortex (CA2) and mesocortex (transentorhinal or perirhinal cortex). Progressive neocortical involvement is in stages 5 and 6. Therefore, stages 4 to 6 may be considered the neuroanatomical basis of progressive cognitive decline in PD.

Unlike Alzheimer's disease (AD), cognitive impairment in PD does not have an amnesic core. As mentioned above, fronto-striatal dopaminergic deficits lead to executive dysfunction. This is probably the more "benign" (non-progressive) form, amenable to treatment with dopaminergic replacement, similar to motor symptoms. The other subtype with a visuo-spatial core is probably the malignant (i.e., progressive) subtype and may be considered as the consequence of tissue damage due to the spread of LBs throughout the stages 4 to 6 (4).

Cognitive impairment in PD can be classified as a continuum divided into four phases: cognitively normal PD (PD-CN), PD with subjective cognitive decline, PD with mild cognitive impairment (PD-MCI), and PD with dementia (PD-D) (1). Recent studies aim to identify PD patients with increased risk of cognitive decline. Structural magnetic resonance imaging (MRI) studies demonstrated that PD-D and PD-MCI patients have brain atrophy in the parietal, occipital, temporal, and frontal lobes and in the hippocampus, amygdala, caudate, putamen, thalamus, and substantia innominata (5, 6). Pagonabarraga et al. (2013) reported linear and progressive cortical thinning in the entorhinal cortex, anterior temporal pole, parahippocampal gyrus, fusiform gyrus, banks of the superior temporal sulcus, lingual gyrus, cuneus, and precuneus across PD cognitive impairment continuum (7). All of these studies to date have used cortical thickness analysis (CTA) and voxel-based morphometry to assess brain atrophy, by means of cortical and subcortical volume and thickness measurements, in PD cognitive impairment continuum. Cortical thickness analysis and voxel-based morphometry are computer-aided quantitative techniques that facilitate the automated assessment of neuroimaging data. These methods allow for the measurement of cortical and subcortical volumes and thicknesses, helping to explore atrophy patterns specific to various diseases, particularly neurodegenerative disorders. While these techniques are highly beneficial for research purposes, they are not appropriate for use in clinical settings as they are very time-consuming. During visual rating, experts can make a more holistic assessment by correlating MRI images with the patient's clinical history, age, symptoms and other factors. Automated methods do not directly take these contextual factors into account.

For this reason, visual rating scales (VRS) have been introduced into clinical practice for assessing atrophy in the diagnosis and follow-up of primary neurodegenerative diseases. Scheltens et al. (1992) developed the first VRS by objectifying the measurement of hippocampal atrophy by assessing medial temporal lobe (MTL) atrophy in Alzheimer's disease (8). By 2011, Koedam et al. (2011) proposed the posterior atrophy (PA) score, which measures posterior cortical atrophy (9). Other VRSs have been described in subsequent studies that assess anterior temporal for semantic dementia and orbitofrontal, anterior cingulate, and fronto-insular atrophy for behavioral variant frontotemporal dementia (10-14). Harper et al. (2016) investigated the effectiveness of VRSs for the differential diagnosis of dementia in 184 patients with a post-mortem diagnosis of dementia and stated that the use of VRSs is quick and easy to learn and can be applied in less than 3 minutes (15). They also emphasized that VRSs can be a time-saving and diagnostically helpful tool in the routine practice of clinicians without neuroradiology expertise. To date, only one study combined six VRSs to assess global brain atrophy in PD, reporting a negative correlation between the total VRS score and the brain volume, but regional atrophy patterns were not evaluated in their study (16).

The present study analyzes magnetic resonance imaging (MRI) data of a previous study, which was designed to investigate the multimodal MRI signatures of cognitive impairment in PD, with two papers published so far (17, 18). The first paper reported arterial spin labeling (ASL) MRI (17) and the second paper reported proton magnetic resonance spectroscopic imaging (1H-MRSI) (18) findings in the PD cognitive impairment continuum. Both papers commonly revealed "posterior cortical changes" in the forms of hypoperfusion and metabolic abnormalities. In this study, we aim to evaluate regional cortical atrophy patterns using VRS corroborated by CTA in PD-MCI and PD-CN patients, with the hypothesis that we will see similar "posterior cortical changes".

METHODS

Participants

All participants provided written informed consent to the main study according to a protocol approved by the Local Ethics Committee of Istanbul University, Istanbul Faculty of Medicine, per the Declaration of Helsinki. In total, 37 right-handed PD patients (18 PD-CN, 19 PD-MCI) diagnosed with idiopathic PD according to the UK Parkinson's Disease Society Brain Bank Diagnostic Criteria at the Istanbul University, Faculty of Medicine, Behavioral Neurology and Movement Disorders Unit were included in the study. The Unified Parkinson's Disease Rating Scale (UPDRS) was applied to all PD patients. Patients with motor symptoms severe enough to cause motion artifact during imaging, a history of any neuropsychiatric diseases other than PD, or a Geriatric Depression Scale (GDS) score of >14 were excluded from the study. For the PD-MCI diagnosis, Movement Disorder Society (MDS) Level I diagnostic criteria were used (19). Accordingly, Addenbrooke's Cognitive Examination-Revised (ACE-R) cut-off score of 83 was used for PD-CN (≥ 83) and PD-MCI distinction (20).

Neuropsychological Battery

ACE-R, which includes Mini-Mental State Examination (MMSE), was used as a screening test. A neuropsychological test battery, including the Stroop Task, Wisconsin Card Sorting Test (WCST), the Benton's Judgment of Line Orientation Test (JLO), and the Symbol-Digit Modalities Test (SDMT), was used. All neuropsychological tests were performed at the on period of the patients with PD.

MRI Acquisition

All MRI data were acquired using a 32-channel SENSE coil on a 3T clinical MR scanner (Phillips, Achieva, Best, Netherlands) installed at the Istanbul University Hulusi Behçet Life Sciences Research Laboratory Neuroimaging Unit. High-resolution anatomical MR images were acquired at the axial plane aligned with the anterior commissure-posterior commissure line using a T1-weighted 3D Turbo Field Echo (TFE) sequence. The scan time was 5 minutes and 55 seconds (repetition time (TR) = 8.4 ms, echo time (TE) = 3.9 ms, flip angle = 8°, number of slices = 180, slice thickness = 1 mm (without gap), voxel size = 1 mm³, and field of view (FOV) = 250 mm).

Visual Rating

The VRS of each participant was determined separately by one expert neurologist (with 8 years of experience, ZY) and one professor of neurology (with 33 years of experience, HG), both specialized in behavioral neurology and both specially trained for VRSs, who were blinded to all clinical information. T1-weighted MRI images were inspected at the axial, coronal and sagittal views. For each patient, the posterior cingulate sulcus (PCS) and the parieto-occipital sulcus (POS) posterior atrophy (PA), the olfactory sulcus (OS) for the orbitofrontal cortex, the anterior cingulate sulcus (ACS) for the anterior cingulate cortex, the circular insular sulcus (Ins) for the fronto-insular cortex, the anterior temporal lobe (ATL), and medial temporal lobe (MTA) were bilaterally evaluated. OS, ACS, Ins, and PA were scored Likert-type between 0-3 (0: no atrophy, 3: severe

atrophy), ATL and MTA were scored Likert-type between 0-4 (0: no atrophy, 4: severe atrophy).

Processing of Structural MRI Data

FreeSurfer (v6.0), which is an open-source software widely used for morphometric analysis of anatomical MRI data enabling surface-based analysis by generating cortical surface models, was used for vertex-wise CTA (21) MRI data of all participants were analyzed using the standard recon-all pipeline. The implemented processing stream included: the removal of nonbrain tissue, transformation to the Talairach reference space and segmentation into the gray and white matter (22), tessellation of the gray matter and white matter boundary, automated topology correction; intensity normalization, and subvoxel representation of the gray matter/white matter boundary and pial surfaces (22, 23). Cortical thickness (CT) was calculated as the shortest distance between the previous surfaces at each vertex (23). Cortical maps were smoothed using a circularly symmetric Gaussian kernel across the surface with a full-width-half-maximum (FWHM) of 15 mm. The general linear model (GLM) was used to determine the cortical thickness differences between the PD-CN and PD-MCI groups.

Statistical Analysis

All demographic, clinical, neuropsychological, and visual rating data were compared using either the independent sample t-test, the Mann-Whitney U test, or the chi-square test according to different variable types using the SPSS software package (version 26.0). Continuous variables that conformed to the normal distribution were presented as mean \pm standard deviation, and the non-normally distributed continuous variables were expressed as median (interquartile range, IQR). Neuropsychological test scores were adjusted for age, sex, and education. The statistical significance was set at two-tailed $p < 0.05$. Interrater reliability was tested using Cohen's weighted kappa, and the associated 95% confidence intervals (CI) were reported. In between-group VRS comparisons, false discovery rate (FDR) correction was used to correct for multiple comparisons at $p < 0.05$, and Cohen's d effect sizes were calculated for all differences. The cut-off value estimation of significant VRS score was conducted through

a Receiver Operating Characteristics (ROC) curve analysis.

GLM analysis, which assesses vertex-wise differences in CT between the two groups, was conducted first for the whole brain and then for three bilateral posterior cortical regions (cuneus, parieto-occipital sulcus, and precuneus) based on Destrieux atlas (24). The specific choice of posterior cortical regions was based on VRS results. To compare cortical thickness data at the group level, a vertex-based general linear model (GLM) analysis was performed using FreeSurfer software. This was used to test for linear relationships between cortical thickness measured for each vertex and independent variables. Firstly, cortical surface models were created for each participant by means of the standard FreeSurfer pipeline. This involved segmenting T1-weighted MRI images, reconstructing cortical surfaces, and registering all surfaces in the standard fsaverage space with equal vertex numbers. After this process, the values of the cortical thickness in each vertex were calculated. The GLM for group comparisons defined cortical thickness values at the vertex level as the dependent variable and group as the independent variable. The relationships between cortical thickness values for each vertex and the independent variables were included in the model equation. To exclude possible effects, age, sex, education level, and the mean levodopa equivalent daily dose (LEDD) were added as covariates in the GLM analysis. To correct for multiple comparisons, a non-parametric cluster-wise Monte Carlo simulation with 10,000 iterations was performed. The vertex-wise threshold was set at $p < 0.001$ for the simulation and clustering, and the clusters were considered as significant if they survived a cluster-wise probability of $p < 0.05$.

RESULTS

There were no statistically significant differences between the PD-CN and PD-MCI groups regarding age, gender, years of education, disease duration, and geriatric depression scores. However, the UPDRS-III scores and the LEDD of the PD-MCI group were higher than those of the PD-CN group. The PD-MCI group had a lower ACE-R total score and sub-scores of all five domains, except the attention/orientation domain. The performance of the PD-MCI group was also worse in terms of the BLO total

Table 1. Demographic, clinical, and neuropsychological features of the study groups

	PD-CN (n = 18)	PD-MCI (n = 19)	Statistics	p
Age (years), mean \pm SD	66.44 \pm 6.85	69.63 \pm 5.07	t(35)= 1.614	0.115
Gender (male/female), n	10 / 8	16 / 3	$\chi^2 = 3.633$	0.057
Education (years), median (IQR)	10.50 (10.00)	5.00 (6.00)	U(35)= 114.00	0.086
Disease duration (years), mean \pm SD	5.31 \pm 2.91	6.00 \pm 3.29	t(35)= 0.679	0.502
UPDRS-III, mean \pm SD	22.61 \pm 8.18	35.16 \pm 14.50	t(35)= 3.216	0.003*
LEDD, mean \pm SD	634.78 \pm 275.45	903.80 \pm 416.31	t(35)= 2.287	0.029*
GDS score, mean \pm SD	5.11 \pm 3.70	5.36 \pm 3.15	t(35)= 0.228	0.821
ACE-R total score, mean \pm SD	88.94 \pm 3.49	77.47 \pm 5.46	t(35)= 7.566	< 0.001*
ACE-R attention/orientation, mean \pm SD	17.67 \pm 0.59	17.26 \pm 1.04	t(35)= 1.453	0.157
ACE-R memory, median (IQR)	21.00 (3.75)	15.00 (7.00)	U(35)= 69.50	< 0.001*
ACE-R fluency, mean \pm SD	10.44 \pm 1.54	8.31 \pm 1.86	t(35)= 3.781	0.001*
ACE-R language, median (IQR)	25.00 (1.25)	23.00 (6.00)	U(35)= 52.00	0.001*
ACE-R visuospatial, mean \pm SD	15.33 \pm 1.14	14.21 \pm 1.44	t(35)= 2.626	0.013*
Stroop test (interference time, s), median (IQR)	60.00 (21.50)	86.00 (54.00)	U(35)= 71.50	0.002*
BLO (total correct), median (IQR)	25.00 (4.00)	20.00 (10.00)	U(35)= 105.00	0.046*
SDMT (total correct), mean \pm SD	29.33 \pm 9.01	16.68 \pm 6.93	t(35)= 4.801	< 0.001*
WCST (perseverative error %), mean \pm SD	20.61 \pm 10.25	27.88 \pm 11.09	t(35)= 2.068	0.046*

SD: Standard deviation, IQR: Interquartile range, PD-CN: Cognitively normal Parkinson's disease, PD-MCI: Parkinson's disease with mild cognitive impairment, ACE-R: Addenbrooke's Cognitive Examination-Revised, s: Second, UPDRS-III: Unified Parkinson's Disease Rating Scale, motor examination, LEDD: Levodopa equivalent daily dose (mg/day), GDS: Geriatric depression scale, BLO: Benton's Line Orientation, SDMT: Symbol-Digit Modalities Test, WCST: Wisconsin Card Sorting Test, t: independent samples t-test χ^2 : Pearson chi-square test, U: Mann-Whitney U-test. *The significance threshold was set at $p < 0.05$.

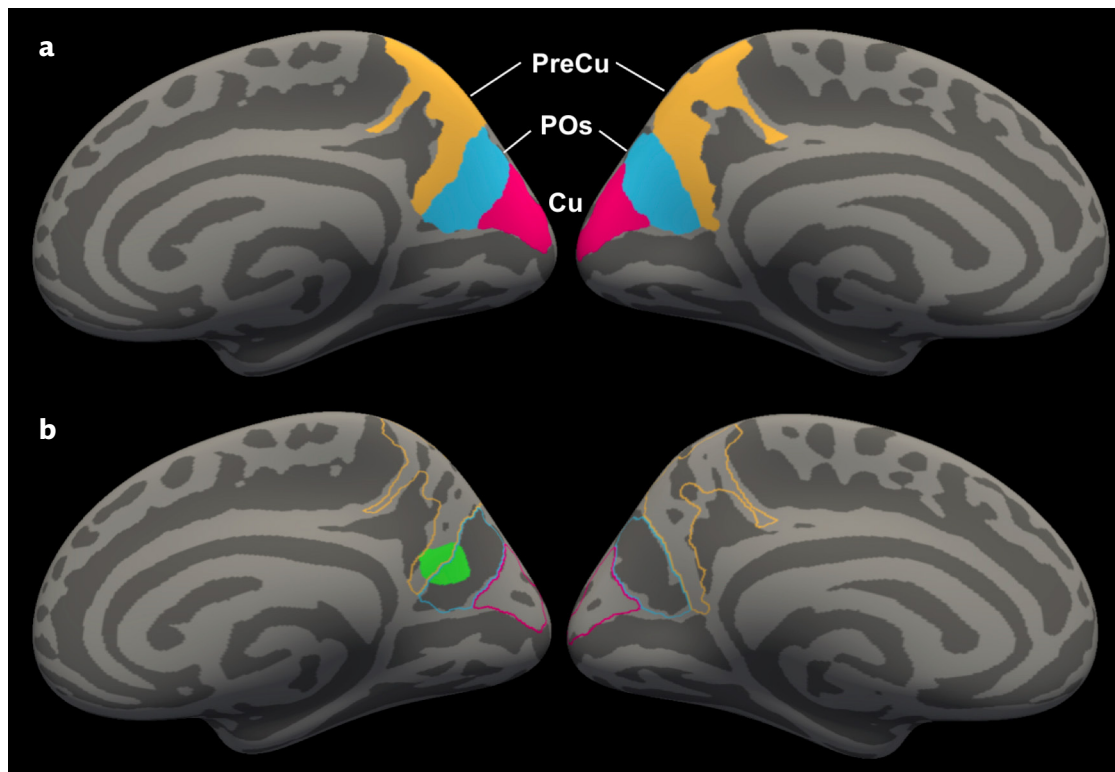


Figure 1. a) Representation of regions defined as a region of interest for CT analysis performed in a restricted area according to VRS results. Pink: cuneus (Cu), blue: parieto-occipital sulcus (POs), and yellow: precuneus (PreCu). **b)** Representation of the cluster showing cortical thinning at the junction of POs and PreCu at the right hemisphere (in green).

correct score, SDMT total correct score, Stroop interference score, and WSCT perseverative error percentage than the PD-CN group (Table 1).

The weighted kappa coefficient was almost perfect for the right orbitofrontal score (0.82 [0.66-0.97]; $p < 0.001$), left orbitofrontal score (0.86 [0.73-0.99]; $p < 0.001$), left anterior cingulate score (0.82 [0.66-0.97]; $p < 0.001$), and right posterior cortex score (0.84 [0.68-0.99]; $p < 0.001$). The weighted kappa coefficient was also substantial for the

right anterior cingulate score (0.80 [0.65-0.94]; $p < 0.001$), right fronto-insular score (0.76 [0.57-0.95]; $p < 0.001$); left fronto-insular score (0.70 [0.49-0.91]; $p < 0.001$), right anterior temporal score (0.77 [0.59-0.93]; $p < 0.001$), left anterior temporal score (0.79 [0.65-0.94]; $p < 0.001$), right medial temporal score (0.70 [0.46-0.93]; $p < 0.001$), left medial temporal score (0.71 [0.50-0.91]; $p < 0.001$) and left posterior cortex score (0.77 [0.61-0.97]; $p < 0.001$).

Table 2. Comparison of visual rating scales between the PD-CN and PD-MCI groups

Visual Rating Scale	PD-CN (n = 18)	PD-MCI (n = 19)	t	P_{FDR}^*	d
R Orbitofrontal	0.61 ± 0.61 [0 - 2]	1.05 ± 0.71 [0 - 2]	2.035	0.343	0.66
L Orbitofrontal	0.67 ± 0.69 [0 - 2]	1.00 ± 0.75 [0 - 2]	1.413	0.581	0.48
R Anterior cingulate	0.67 ± 0.59 [0 - 2]	0.84 ± 0.76 [0 - 2]	0.776	0.563	0.26
L Anterior cingulate	0.78 ± 0.81 [0 - 2]	1.05 ± 0.78 [0 - 2]	1.053	0.600	0.36
R Fronto-insular	1.05 ± 0.62 [0 - 3]	1.11 ± 0.83 [0 - 2]	0.243	0.809	0.08
L Fronto-insular	1.28 ± 0.67 [0 - 3]	1.47 ± 0.61 [0 - 2]	0.930	0.628	0.31
R Anterior temporal	0.61 ± 0.78 [0 - 2]	0.79 ± 0.42 [0 - 1]	0.875	0.541	0.30
L Anterior temporal	0.56 ± 0.62 [0 - 2]	0.79 ± 0.63 [0 - 2]	1.141	0.734	0.39
R Medial temporal	0.28 ± 0.57 [0 - 2]	0.47 ± 0.70 [0 - 2]	0.930	0.558	0.31
L Medial temporal	0.39 ± 0.61 [0 - 2]	0.63 ± 0.68 [0 - 2]	1.139	0.614	0.38
R Posterior atrophy	1.17 ± 0.62 [0 - 2]	1.84 ± 0.69 [1 - 3]	3.134	0.042	1.06
L Posterior atrophy	1.50 ± 0.71 [1 - 3]	1.63 ± 0.68 [1 - 3]	0.575	0.663	0.19

Data are presented as mean ± standard deviation [range]. PD-CN: Cognitively normal Parkinson's disease, PD-MCI: Parkinson's disease with mild cognitive impairment, t: independent samples t-test, FDR-corr: False discovery rate correction, d: Cohen's d (effect size), *FDR corrected threshold set at $p < 0.05$.

In the between-group comparison of VRS, the right PA score of the PD-MCI group was higher than that of the PD-CN group ($p_{FDR-corr} = 0.042$, Cohen's $d = 1.06$) (Table 2).

No statistically significant difference was found between the two groups in the vertex-wise CT analysis of the whole brain. On the other hand, CT analysis involving the bilateral posterior cortex showed cortical thinning in an area covering the right parieto-occipital sulcus and precuneus in the PD-MCI group compared to the PD-CN group (Max. $T = 6.171$, $P = 0.0006$, $MNI_x, y, z = 11.0, -62.2, 25.4$) (Figure 1b).

The ROC curve revealed that the AUC was 0.75 (95% CI, 0.57–0.93), showing a good association between the PD-MCI and the right PA scores (Figure 2). The cut-off for the right PA VRS score was set as ≥ 2 . This cut-off showed the optimal sensitivity (68%) and specificity (72%). PA score > 0 had a 100% sensitivity, and PA score = 3 had a 100% specificity (Table 3). A cut-off points of ≥ 2 for the right PA score indicates optimal performance with a sensitivity of 68% and a specificity of 72%. This means that 68% of people with PD-MCI are correctly identified, but 32% are classified as false negative. Similarly, 72% specificity indicates that 72% of people without PD-MCI are correctly identified, but 28% are classified as false positives.

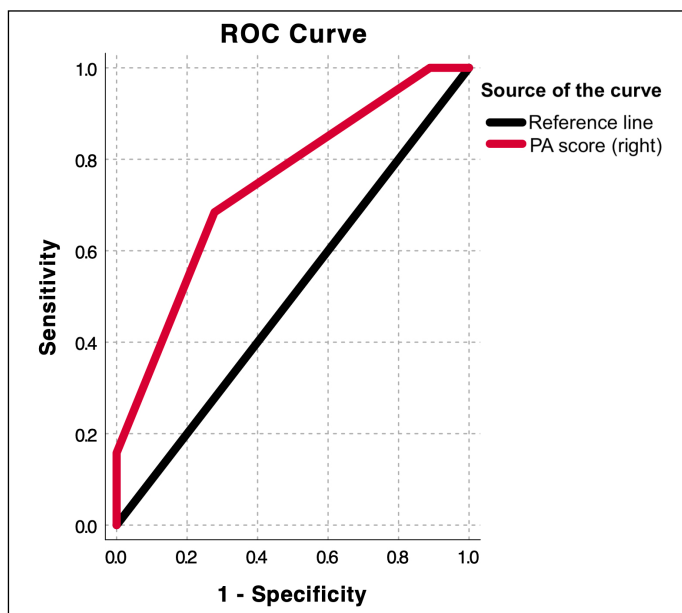


Figure 2. The ROC curve for right posterior atrophy (PA) score.

Table 3. Right posterior atrophy VRS scores of two patient groups

Scores	0	1	2	3
PD-CN	2	11	5	0
PD-MCI	0	6	10	3

PD-CN: Cognitively normal Parkinson's disease; PD-MCI: Parkinson's disease with mild cognitive impairment; n: number of subjects; VRS: Visual rating scale.

DISCUSSION

We evaluated the regional cortical atrophy pattern via VRS between PD-MCI patients and PD-CN patients. The PD-CN group outperformed the PD-MCI group in almost every neuropsychological measure, with the exception of the ACE-R Attention/Orientation subscore. Although whole

brain cortical thickness analysis showed no difference between the two groups, in the PD-MCI group, not only the VRS scores of right posterior atrophy (combined POS and pCS evaluation) were higher, but also the CT analysis revealed significantly thinner POS and precuneus. A right PA-VRS score of ≥ 2 became the optimal cut-off, with > 0 having the best sensitivity and =3 best specificity (both 100%). These new findings add to our previous studies on the same cohort mentioned in the last paragraph of the introduction section, which we summarized as "posterior cortical-type change."

Lin and colleagues were the first to assess global cortical atrophy in PD by using VRS. They combined the 6 VRS and calculated a total VRS score. They showed that the total VRS score was significantly correlated with quantitative brain volume. They also showed the global atrophy detected by VRS is associated with non-motor symptoms, especially depression. They did not report a specific regional atrophy pattern (16).

Several studies on brain atrophy in PD cognitive impairment continuum showed a linear atrophy pattern from PD-CN to PDD, particularly in parieto-temporal and prefrontal cortices, and parietal-temporal cortex, prefrontal cortex, hippocampus, and amygdala atrophy in PD-MCI have been reported (5). Pagonabarraga et al. (2013) observed a cortical thinning pattern including the entorhinal cortex, anterior temporal pole, parahippocampal cortex, fusiform gyrus, banks of the superior temporal sulcus, lingual gyrus, cuneus and precuneus in PD-MCI patients and they showed that this pattern is linear and progressive from PD-CN to PDD (7). Weintraub et al.'s (2012) study showed that cognitive decline in PD is associated with an atrophy pattern including the hippocampus, medial temporal lobe, and parieto-temporal cortex, as in AD, and they suggested that this AD pattern of atrophy might be a biomarker for cognitive decline in PD (25). Hippocampal volume has been demonstrated as a significant predictive factor for the progression from PD-NCI to PD-MCI and PD-MCI to PDD (26). Although hippocampal atrophy has been reported in structural MRI studies, studies in other imaging modalities such as MRS, ASL-MRI, functional connectivity MRI, or FDG-PET showed metabolic abnormalities, hypoperfusion, decreased connectivity of intrinsic connectivity networks or hypometabolism predominantly in posterior cortical areas (5, 17, 18, 27). Furthermore, it can be claimed that hippocampal dysfunction does not play an essential role in the memory impairment of PD patients, whose recognition memory is largely intact in contrast to AD patients' "limbic-type" or hippocampal recognition memory impairment. The acquisition and retrieval (free-recall) deficits of memory-impaired PD patients are commonly attributed to poor attentional/dysexecutive mechanisms rather than a primary impairment of the episodic memory neural network (i.e., the Papez circuit) (28).

Braak and Braak's NFT spread in AD and Braak et al.'s LB spread in PD overlaps in their so-called transentorhinal cortex (TEC), better known as the perirhinal gyrus (PRG), corresponding to Brodmann areas 35 and 36. The former is their stage I, and the latter is stage 4, stages 1-3 being non-cortical, caudo-rostral brainstem progression (3, 29, 30). However, interestingly, AD propagation continues by walking over the steps of first the intrinsic hippocampal circuit and then the Papez circuit resulting in a progressive amnesic syndrome. In contrast, PD spread largely neglects this limbic-paralimbic route and jumps over the visual neocortex resulting in a progressive visuo-spatial syndrome. Commenting on the subject matter, Braak and Del Tredici interpreted the common initial cortical involvement in TEC by the induction of protein misfolding via the synaptic contact of the long axons of non-thalamic nuclei with diffuse cortical projections (31). Braak et al. (2011) had already extended their staging of AD tau propagation, adding pre-NFT (Stage I-VI) stages a-c and 1a, 1b. Locus coeruleus is the core structure here containing Gallyas-negative (non-argyrophilic), non-fibrillary, hence soluble hyperphosphorylated tau, named "pre-tangle" (30). This very early involvement is accompanied

by the involvement of other “non-thalamic” nuclei with diffuse cortical projections over the course of these pre-NFT stages. Having reached the cortex through the involvement of TEC, they speculated a further cortical spread along the interconnected pathways via anterograde and retrograde axonal transport as the likely mechanism.

Although innovative for the common initiation of cortical pathology, their discussion does not provide an explanation for the divergence of trajectories of spread after TEC. Additionally, for AD, they do not discuss the potential roles of amyloid and inflammation in NFT spread. There is probably more than one mechanism for NFT tau propagation in AD. This was already promulgated in a recent paper, which stated that one mechanism is indeed spread over to distant cortical sites via axonal connections; however, the second one is replication around a seed and then being taken over by the neighboring neuron by endocytosis (32). The authors also claimed that although both are operative during the initial stages after Braak & Braak III, replication becomes the sole mechanism for neocortical propagation. Why after III? A number of other recent papers shed light on this question. Insel et al., using three large cohorts consisting of individuals with pre-clinical AD, showed that with the presence of elevated A β 42, the inferior temporal cortex (ITCx) showed the largest effect size, followed by the fusiform gyrus, and they concluded that while the medial temporal structures “play a central role in the early appearance of tau, it may be the inferior temporal cortex that is the critical region for rapid tau accumulation in preclinical Alzheimer’s disease” (33). Lee et al. (2022) also reported two mechanisms of tau propagation. The first is the lateral entorhinal cortex (interconnected with TEC) that “is subject to remote, connectivity-mediated amyloid-beta/tau interactions linked to initial tau spreading.” (34). The second is the inferior temporal cortex, the site of initial A β 42/Tau co-localization, “as the region featuring the greatest local amyloid-beta/tau interactions and a connectivity profile well suited to accelerate tau propagation.” Finally, Pascoal and colleagues (2021) using PET ligands separately for A β , tau aggregates, and microglial activation, showed that the neocortical propagation of tau and the consequent evolution of AD dementia is largely driven by microglial activation (35). These findings suggest a local propagation to inferior posterior cortices, probably via a joint mechanism of replication and spread pathways made easier to follow by both compact amyloid plaques and microglial activation induced by them.

However, in PD, LBs, lacking these extra aides seems still use the distant pathway spread mechanisms, at least for reaching the precuneus and POS we found atrophied in this study. ITCx and these posteromedial cortical structures are interconnected by the fifth division of the cingulum bundle (CING V) (36). Recently, fornix integrity was proposed as a structural connectivity imaging (e.g., diffusion tensor imaging – DTI) marker for progressive cognitive decline in AD, named “the fornix sign.” (37). Our aim is to proceed this project to find a similar imaging biomarker for PD cognitive decline. A “CING V sign” would be a perfect sign.

This study has a number of limitations. The main limitation of our research is a small sample size, which will undoubtedly affect how broadly applicable our conclusions may be. Moreover, a secondary constraint that results in a less than ideal degree of accuracy in classification accuracy is the use of level I diagnostic criteria to define PD-MCI. Lastly, our study involved a cross-sectional comparison of two patient groups that prevents identification of causation, therefore future longitudinal assessments are crucial.

CONCLUSION

In conclusion, this study found structural alterations, specifically in posterior cortical areas that we had already shown in the same cohort with different neuroimaging methods, revealing decreased

perfusion and increased metabolic abnormalities. VRS, an easy and brief method to use by clinicians in routine clinical practice, almost mirrored the findings of the more sophisticated and time-consuming cortical thickness analysis. Posterior cortical atrophy, as revealed by VRS, may be a specific practical imaging marker of PD-MCI, as the VRS medial temporal atrophy has already been established for the typical Alzheimer’s disease.

Acknowledgment: We would like to thank Dilek Betül Arslan, Sevim Cengiz, and Zeynep Tufekcioglu for their contributions to data collection. EE received a yearly doctoral stipend (57140539) from the DAAD (German Academic Exchange Service). This study was presented as an oral presentation at the 12th National Alzheimer Congress, held in Eskisehir, Turkey, from October 29th to November 2nd, 2022.

Ethics Approval: The study was approved by the Clinical Research Ethics Committee of Istanbul University, Istanbul Faculty of Medicine (Protocol Number: 2022/1494).

Participant Consent: The participants were informed about the research and their written consents were obtained before the data acquisition.

Author Contributions: Concept - UA, ZY, HG; Design - UA, ZY, HG; Supervision - BB, HH, EOI, TD, HG; Resources - EOI, TD; Data Collection and/or Processing - AK, EE, BB, HH; Analysis and/or Interpretation - UA, ZY, AK, EE, BB, HH, EOI, TD, HG; Literature Review - UA, ZY, HG; Writing - UA, ZY, EE, AK; Critical Review - BB, HH, EOI, TD, HG.

Competing Interests : The authors report no competing interests.

Funding: This study was funded by the Scientific and Technological Research Council of Turkey (TUBITAK) grant #115S219 and the Istanbul University Research Projects Unit grant #TSA-2022-39128.

REFERENCES

- Aarsland D, Batzu L, Halliday GM, Geurtsen GJ, Ballard C, Ray Chaudhuri K et al. Parkinson disease-associated cognitive impairment. *Nat Rev Dis Primers* 2021;7:47. [Crossref]
- Pfeiffer RF. Non-motor symptoms in Parkinson’s disease. *Parkinsonism Relat Disord* 2016;22:S119-S122. [Crossref]
- Braak H, Del Tredici K, Rub U, de Vos RA, Jansen Steur EN, Braak E. Staging of brain pathology related to sporadic Parkinson’s disease. *Neurobiol Aging* 2003;24:197-211. [Crossref]
- Janvin CC, Larsen JP, Aarsland D, Hugdahl K. Subtypes of mild cognitive impairment in Parkinson’s disease: progression to dementia. *Mov Disord* 2006;21:1343-1349. [Crossref]
- Delgado-Alvarado M, Gago B, Navalpotro-Gomez I, Jimenez-Urbieta H, Rodriguez-Oroz MC. Biomarkers for dementia and mild cognitive impairment in Parkinson’s disease. *Mov Disord* 2016;31:861-881. [Crossref]
- Ay U, Yildirim Z, Erdogdu E, Kicik A, Ozturk-Isik E, Demiralp T ve ark. Shrinkage of olfactory amygdala connotes cognitive impairment in patients with Parkinson’s disease. *Cogn Neurodyn* 2023;17:1309-1320 [Crossref]
- Pagonabarraga J, Corcuera-Solano I, Vives-Gilbert Y, Llebaria G, Garcia-Sanchez C, Pascual-Sedano B et al. Pattern of regional cortical thinning associated with cognitive deterioration in Parkinson’s disease. *PLoS One* 2013;8:e54980. [Crossref]
- Scheltens P, Leys D, Barkhof F, Huglo D, Weinstein HC, Vermersch P et al. Atrophy of medial temporal lobes on MRI in “probable” Alzheimer’s disease and normal ageing: diagnostic value and neuropsychological correlates. *J Neurol Neurosurg Psychiatry* 1992;55:967-972. [Crossref]
- Koedam EL, Lehmann M, van der Flier WM, Scheltens P, Pijnenburg YA, Fox N et al. Visual assessment of posterior atrophy development of a MRI rating scale. *Eur Radiol* 2011;21:2618-2625. [Crossref]
- Ambikairajah A, Devenney E, Flanagan E, Yew B, Mioshi E, Kiernan MC ve ark. A visual MRI atrophy rating scale for the amyotrophic lateral sclerosis-frontotemporal dementia continuum. *Amyotroph Lateral Scler Frontotemporal Degener* 2014;15:226-234. [Crossref]
- Davies RR, Kipps CM, Mitchell J, Kril JJ, Halliday GM, Hodges JR. Progression in frontotemporal dementia: identifying a benign behavioral variant by magnetic resonance imaging. *Arch Neurol* 2006;63: 1627-1631. [Crossref]
- Davies RR, Scahill VL, Graham A, Williams GB, Graham KS, Hodges JR. Development of an MRI rating scale for multiple brain regions: comparison with volumetrics and with voxel-based morphometry. *Neuroradiology* 2009;51:491-503. [Crossref]

13. Hornberger M, Savage S, Hsieh S, Mioshi E, Piguet O, Hodges JR. Orbitofrontal dysfunction discriminates behavioral variant frontotemporal dementia from Alzheimer's disease. *Dement Geriatr Cogn Disord* 2010;30:547-552. [\[Crossref\]](#)
14. Kipps CM, Davies RR, Mitchell J, Kril JJ, Halliday GM, Hodges JR. Clinical significance of lobar atrophy in frontotemporal dementia: application of an MRI visual rating scale. *Dement Geriatr Cogn Disord* 2007;23:334-342. [\[Crossref\]](#)
15. Harper L, Fumagalli GG, Barkhof F, Scheltens P, O'Brien JT, Bouwman F et al. MRI visual rating scales in the diagnosis of dementia: evaluation in 184 post-mortem confirmed cases. *Brain* 2016;139:1211-1225. [\[Crossref\]](#)
16. Lin Y, Fu Y, Zeng YF, Hu JP, Lin XZ, Cai NQ et al. Six Visual Rating Scales as A Biomarker for Monitoring Atrophied Brain Volume in Parkinson's Disease. *Aging Dis* 2020;1:1082-1090. [\[Crossref\]](#)
17. Arslan DB, Gurvit H, Genc O, Kicik A, Eryurek K, Cengiz S et al. The cerebral blood flow deficits in Parkinson's disease with mild cognitive impairment using arterial spin labeling MRI. *J Neural Transm (Vienna)* 2020;127:1285-1294. [\[Crossref\]](#)
18. Cengiz S, Arslan DB, Kicik A, Erdogdu E, Yildirim M, Hatay GH et al. Identification of metabolic correlates of mild cognitive impairment in Parkinson's disease using magnetic resonance spectroscopic imaging and machine learning. *MAGMA* 2022;35:997-1008. [\[Crossref\]](#)
19. Litvan I, Goldman JG, Troster AI, Schmand BA, Weintraub D, Petersen RC et al. Diagnostic criteria for mild cognitive impairment in Parkinson's disease: Movement Disorder Society Task Force guidelines. *Mov Disord* 2012; 27:349-356. [\[Crossref\]](#)
20. Uysal-Canturk P, Hanagasi HA, Bilgic B, Gurvit H, Emre M. An assessment of Movement Disorder Society Task Force diagnostic criteria for mild cognitive impairment in Parkinson's disease. *Eur J Neurol* 2018;25:148-153. [\[Crossref\]](#)
21. Ay U, Kizilates-Evin G, Bayram A, Kurt E, Demiralp T. Comparison of FreeSurfer and CAT12 Software in Parcel-Based Cortical Thickness Calculations. *Brain Topogr* 2022;35:572-582. [\[Crossref\]](#)
22. Dale AM, Fischl B, Sereno MI. Cortical surface-based analysis. I. Segmentation and surface reconstruction. *Neuroimage* 1999;9:179-194. [\[Crossref\]](#)
23. Fischl B, Sereno MI, Dale AM. Cortical surface-based analysis. II: Inflation, flattening, and a surface-based coordinate system. *Neuroimage* 1999;9:195-207. [\[Crossref\]](#)
24. Destrieux C, Fischl B, Dale A, Halgren E. Automatic parcellation of human cortical gyri and sulci using standard anatomical nomenclature. *Neuroimage* 2010;53:1-15. [\[Crossref\]](#)
25. Weintraub D, Dietz N, Duda JE, Wolk DA, Doshi J, Xie SX et al. Alzheimer's disease pattern of brain atrophy predicts cognitive decline in Parkinson's disease. *Brain* 2012;135:170-180. [\[Crossref\]](#)
26. Kandiah N, Zainal NH, Narasimhalu K, Chander RJ, Ng A, Mak E et al. Hippocampal volume and white matter disease in the prediction of dementia in Parkinson's disease. *Parkinsonism Relat Disord* 2014; 20:1203-1208. [\[Crossref\]](#)
27. Ay U, Gurvit IH. Alterations in Large-Scale Intrinsic Connectivity Networks in the Parkinson's Disease-Associated Cognitive Impairment Continuum: A Systematic Review. *Arch Neuropsychiatry* 2022;59:S57-S66. [\[Crossref\]](#)
28. Chiaravalloti ND, Ibarretxe-Bilbao N, DeLuca J, Rusu O, Pena J, Garcia-Gorostiaga I et al. The Source of the Memory Impairment in Parkinson's Disease: Acquisition Versus Retrieval. *Mov Disord* 2014;29:765-771. [\[Crossref\]](#)
29. Braak H, Del Tredici K, Bratzke H, Hamm-Clement J, Sandmann-Keil D, Rub U. Staging of the intracerebral inclusion body pathology associated with idiopathic Parkinson's disease (preclinical and clinical stages). *J Neurol* 2001;249:1-5. [\[Crossref\]](#)
30. Braak H, Thal DR, Ghebremedhin E, Del Tredici K. Stages of the pathologic process in Alzheimer disease: age categories from 1 to 100 years. *J Neuropathol Exp Neurol* 2011;70: 960-969. [\[Crossref\]](#)
31. Braak H, Del Tredici K. Potential Pathways of Abnormal Tau and alpha-Synuclein Dissemination in Sporadic Alzheimer's and Parkinson's Diseases. *Cold Spring Harb Perspect Biol* 2016;8:a023630. [\[Crossref\]](#)
32. Meisl G, Hidari E, Allinson K, Rittman T, DeVos SL, Sanchez JS et al. In vivo rate-determining steps of tau seed accumulation in Alzheimer's disease. *Sci Adv* 2021;7:eabh1448. [\[Crossref\]](#)
33. Insel PS, Young CB, Aisen PS, Johnson KA, Sperling RA, Mormino EC et al. Tau positron emission tomography in preclinical Alzheimer's disease. *Brain* 2022;146:700-711. [\[Crossref\]](#)
34. Lee WJ, Brown JA, Kim HR, La Joie R, Cho H, Lyoo CH et al. Regional Abeta-tau interactions promote onset and acceleration of Alzheimer's disease tau spreading. *Neuron* 2022;110:1932-1943. [\[Crossref\]](#)
35. Pascoal TA, Benedet AL, Ashton NJ, Kang MS, Therriault J, Chamoun M et al. Microglial activation and tau propagate jointly across Braak stages. *Nat Med* 2021; 27:1592-1599. [\[Crossref\]](#)
36. Maldonado IL, Parente de Matos V, Castro Cuesta TA, Herbet G, Destrieux C. The human cingulum: From the limbic tract to the connectionist paradigm. *Neuropsychologia* 2020;144:107487. [\[Crossref\]](#)
37. Oishi K, Mielke MM, Albert M, Lyketsos CG, Mori S. The fornix sign: a potential sign for Alzheimer's disease based on diffusion tensor imaging. *J Neuroimaging*. 2012; 22:365-374. [\[Crossref\]](#)